Rhythmic morphology in a microtidal low-energy beach

Anna Mujal-Colilles[1a,*]

anna.mujal@upc.edu

Manel Grifoll[1a]

Albert Falqués[2b]

[1a]Laboratori d'Enginyeria Marítima, Department of Civil and Environmental Engineering, UPC-Barcelona Tech, C/ Jordi Girona, 1-3, 08034 Barcelona, Spain

[2b]Department of Physics, UPC-Barcelona Tech, C/ Jordi Girona, 1-3, 08034 Barcelona

*Corresponding author.

Abstract

Observations of rythmic features along the inner side of the Trabucador barrier beach are coupled to two numerical models to unravel the mechanisms of its formation. The Trabucador is a long (6 Km) narrow (125 m) barrier and microtidal beach at the SW side of the Ebro delta (Catalonia). Its inner side is a low energy beach with a sandy shallow terrace featuring an intricate alongshore rhythmic morphology. Sixteen aerial orthophotos from 1946 to 2014 have been analyzed and complemented with field observations from 1986 to present. This morphology is dynamic but it is usually characterized by: a) long finger transverse bars (LFTB) and b) large scale shoreline undulations (LSSU). The LFTB are thin and elongated with a length of the order of their spacing. They are intertidal and typically attach to the shoreline by a megacusp, commonly opening an anti-clockwise angle of 10°–40° with the shore normal. There can be many, up to 90, with both the mean and the most frequent alongshore spacing in the range 15–25 m. Spectral analysis always shows peaks in this range and sometimes additional peaks in the range 30–65 m that correspond to the spacing between the largest bars with smaller bars in between. The LSSU typically have wavelengths in the range 150–250 m. Their apexes sometimes coincide with the shore attachment of the largest bars but not always. Numerical modelling shows that both features could emerge out of feedbacks between hydrodynamics and morphology during the SW wind events involving a) deflection of the longshore current by the bars combined with the refractive wave focusing and b) gradients in total alongshore sediment transport rate triggering the high-angle wave instability.

Keywords: Long finger transverse bars; Shoreline undulations; Spectral analysis; Alfacs Bay; Low energy beach; High-angle wave instability; Surf zone morphodynamic instabilities

1.1 Introduction

The morphology of sandy coasts, including the shoreline position and the bathymetry of the surf and shoaling zones, quite often displays complex and intriguing patterns. These patterns are sometimes nearly periodic alongshore or at least showing some sort of regularity with an alongshore recurrence length, L, and are then known as *rhythmic coastal morphologies*. Some types have been defined in the literature (Short, 1999; Ribas et al., 2015) but the extreme complexity of beach dynamics and the increasing capacity and frequency of beach monitoring and field observations often challenge their traditional classification (Guillén et al., 2017).

Transverse sand bar systems is one type of those patterns. The term *transverse bar* (TB) is generically applied to sand bars extending perpendicularly to the coast or with an oblique orientation (Shepard, 1952). They usually occur in patches of a few of them up to tens, they are separated by troughs and they are typically attached to the shore. The alongshore spacing, L, is defined as the distance between successive bar crests. With a dominant longshore current they tend to migrate downdrift with migration rates up to 40 m/d (Ribas and Kroon, 2007; Pellón et al., 2014). They sometimes show an asymmetry of their cross-section (the down-current flank being steeper than the up-current flank, Pellón et al., 2014).

Several types of transverse bars have been reported in the literature (see, e.g., Pellón et al., 2014; Ribas et al., 2015). The first ones are *TBR bars*, which are associated to the Transverse Bar and Rip (TBR) state in the standard beach state classification (Wright and Short, 1984). They are typically wide and short-crested and their origin is the merging of the horns of a crescentic bar into the beach. The second type are *medium energy finger bars*, MEFB, which are sometimes observed in open microtidal beaches under medium-energy conditions (Konicki and Holman, 2000; Khabidov, 2001; Ribas and Kroon, 2007) and they always coexist with shore-parallel (or crescentic) bars. They are thin and elongated in contrast with the wider and shorter TBR bars. MEFB are ephemeral (residence time from 1 day to 1 month), attached to the low-tide shoreline or, occasionally, to the shore-parallel bar. They are linked to the

presence of alongshore wave driven current and they are up-current oriented, i.e., their distal tip is shifted up-current with respect to the shore-attachment. Their spacing is in the range $L \approx 15 - 200$ m. Finally, the *long finger transverse bars* type, LFTB, which groups the "large-scale finger bars" and the "low-energy finger bars" of the classification of Pellón et al. (2014). They are characterized by long crests, which are typically larger than the alongshore spacing which may vary in the range $L \approx 10 - 500$ m. They are generally observed to be persistent features in low to medium wave energy system whose foreshore is a very flat terrace (Evans, 1938; Niederoda and Tanner, 1970; Bruner and Smosna, 1989; Falqués, 1989; Gelfenbaum and Brooks, 2003;). The wave focusing caused by topographic refraction by the bars seems to be an essential process to them. Although they are most often observed on microtidal beaches, they may also exist on *meso* and macrotidal coasts (Levoy et al., 2013; Pellón et al., 2014). They tend to be oriented almost perpendicular to the shore or with a small angle.

In addition to surf/shoaling zone bathymetry, the shoreline itself can also display an alongshore rhythmicity in the form of undulations or cuspate shapes. Some of them are linked to transverse bar systems, so that their apexes develop at the shore attachments of the bars and the embayments in between correspond to the troughs in between bars. They are known as *megacusps*. Shorelines may also display undulations at a scale which is larger than surf zone rhythmic bars, i.e., $L \gg X_b$, where X_b is the width of the surf zone. These large scale undulations have typical alongshore wavelengths >1 Km (on open ocean beaches) and are linked to similar undulations in the depth contours well offshore the surf zone. They have been called *Km-scale shoreline sand waves* (Idier and Falqués, 2014).

The origin and driving mechanisms of nearshore alongshore rhythmic patterns have been puzzling scientists for long. Their striking and relatively regular morphology along with its clear characteristic alongshore spacing in spite of the multi-scale high complexity of coastal dynamics suggests that something important occurs in the physics at that particular length scale. A common assumption in the past was that a pre-existing template in the hydrodynamics (currents and/or waves) imprints its particular pattern on the morphology (Holman and Bowen, 1982). Since the feedback from the developing morphology into the hydrodynamics is ignored in this approach these type of explanations have been increasingly discarded (Coco and Murray, 2007). Alternatively, it has been found that rhythmic morphologies can emerge from internal instabilities of the coupling between morphology and hydrodynamics through the sediment transport (Coco and Murray, 2007; Ribas et al., 2015). This has been shown for crescentic bars (Deigaard et al., 1999; Falqués et al., 2000; Calvete et al., 2005; Garnier et al., 2008), transverse bars (Garnier et al., 2006; Ribas et al., 2003, 2012), beach cusps (Coco et al., 2000; Dodd et al., 2008) and Km-scale shoreline undulations (Ashton et al., 2001; Falqués and Calvete, 2005; van den Berg et al., 2012; Kaergaard and Fredsoe, 2013), and is known as the *self-organization theory*.

Checking the self-organization explanation for alongshore rhythmic features needs frequent and detailed bathymetric surveys along with measurements of currents and waves during the time where the features are incipient. Since this type of information is very scarce, providing detailed and high quality data on rhythmic morphology development and dynamics is strongly valuable. The southwestern flank of the Ebro delta (Catalonia) features a long spit or barrier beach called Trabucador beach, which separates the Alfacs Bay from the open Mediterranean Sea. The inner side of the Trabucador beach commonly displays transverse bars and megacusps with a typical alongshore spacing of tens of m. At the same time, aerial photos (available since 1946) also show the presence of larger scale shoreline undulations, up to ~250 m. The Trabucador beach can be considered as "low-energy" since it is sheltered from the open sea waves. A preliminary description of this system was done by Falqués (1989).

There are in the literature many theoretical studies on rhythmic surf zone bars and on large scale shoreline undulations. However, the application of such studies to specific features observed in nature is much scarcer. Moreover, there are no studies of rhythmic surf zone bars coexisting with large scale undulations. Therefore, the Trabucador beach case has provided a unique opportunity of studying, for the first time, both types of features in coexistence and from both views: observations and modelling.

The primary objective of the present paper is a more thorough description and characterization of the rhythmic morphology in this beach. We mainly use spectral analysis of the shorelines from aerial orthophotos during the period 1946–2014 along with occasional field observations by one of the authors during the period 1986–2014. We hypothesize that their morphology and the length scales are largely self-organized and the second objective is investigating the physical mechanisms driving its formation and dynamics by means of numerical modelling.

~~2.~~2 Study Area and morphology

~~2.1.~~2.1 Geographical setting and meteo-oceanographic conditions

The Ebro delta is located in the western Mediterranean sea, NE of the Iberian peninsula, in Catalonia (see Fig~~ure~~. 1). As a result of the interaction of the river and marine dynamics (Jiménez et al., 1997), the present day delta extends around 25 km offshore and has an area of about 325 Km^2. On the lateral margins it features two spits, one trending to the NW (El Fangar), another trending to the SW and consisting of the Trabucador barrier beach and La Banya peninsula. Between the southwestern spit (Trabucador and La Banya) and the mainland, there is a semi-enclosed bay called Alfacs bay. It is nearly rectangular about 16 km long and 4 km wide, with an average depth of about 4 m (6.5 in the center of the bay). The Alfacs bay can be geomorphologically classified as a bar-built semi-enclosed lagoon formed as the result of the reworking of an abandoned lobe of the first Ebro River mouth, directed to the south by waves (Pritchard, 1952, Nienhuis et al., 2017). The bay receives considerable amount of freshwater from rice crops (of the order of $10 m^3 \cdot s^{-1}$ during opened channels) leading an almost stable stratification throughout the year. So, according to conductivity, temperature and density profilers during different periods, the semi-enclosed lagoon is classified hydrodynamically as a salt-wedge estuary (Llebot et al., 2014; Cerralbo et al., 2015a). The bed is made of silt and

clay (largest percentages in the middle of the bay) (Palacin et al., 1991). However, next to the inner side of the Trabucador barrier beach there is a sandy and shallow shelf, see Figure 2, that is composed of fine sand with $D_{50} \approx 0.15 - 0.3$ mm (Falqués, 1989). This shelf deepens from 0 to roughly 0.7 m within about 125 m width and, presumably, it has been built out of sediments from the outer side of the beach during overwash events.

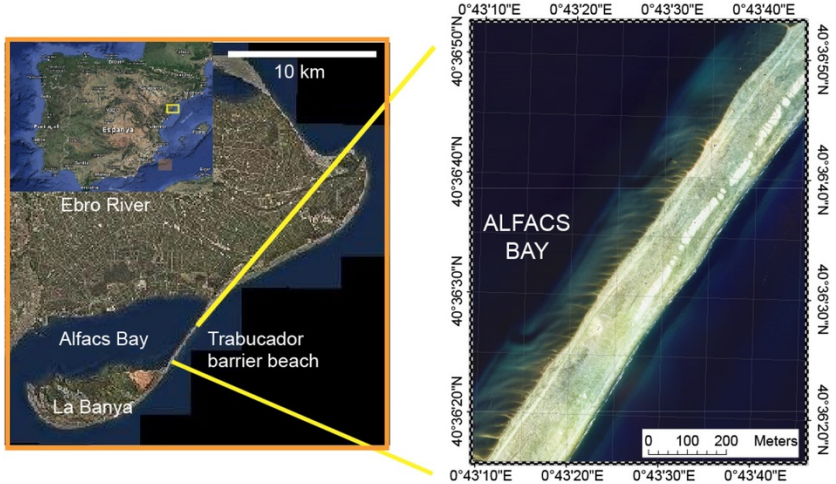

~~Figure 1~~**Fig. 1** Left: the Ebro delta with the Trabucador beach (in yellow). Other geographical locations mentioned in the text are also shown. Right: The Trabucador barrier beach in 2012. The shallow shelf with the transverse bars can be seen at the inner side. Source: ICGC. (For interpretation of the references to colour in this figure legend, the reader is referred to the web version of this article.)

alt-text: Fig. 1

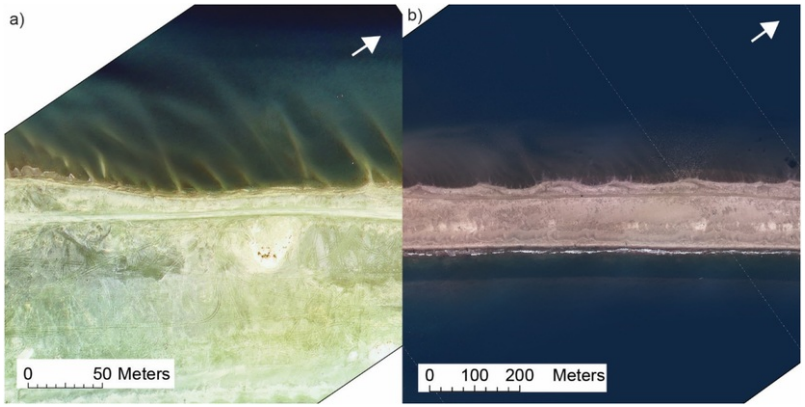

~~Figure 2~~**Fig. 2** a) Detailed view of the transverse bar system in 2012. b) View of the inner Trabucador beach in 2013 where the large scale undulations are visible. Source: ICGC. White arrow represents the North.

alt-text: Fig. 2

The wind regime in the Ebro Delta is characterized by the prevalence of North-Westerly winds during autumn and winter and onshore/offshore winds (daily sea-breeze) during summer (Cerralbo et al., 2015b; Grifoll et al., 2016). Using one-year observed wind data, Grifoll et al. (2015) estimate the monthly percentage of time of NW winds: during winter this percentage was about 80 % decreasing during summer to 20 %. See breeze occurs daily during summer and in a lesser extend during spring. North-Westerly winds arise 15 $m \cdot s^{-1}$ and typical values of sea-breeze are of the order of 8 $m \cdot s^{-1}$. According to the wind climate, and because this beach is sheltered, waves are expected to be very small in comparison to the open-sea side of the Trabucador.

This beach is microtidal, with tidal range ~0.25 m, but sea-level oscillation due to seiches activity is relevant (Cerralbo et al., 2014) with amplitudes of ~~more than~~ ≥0.5 m measured within the bay with characteristic periods of 1 h and 3 h (0th and 1st seiche modes). The water circulation in Alfacs bay at short temporal scales (orders of hours) is dominated by the local wind and the occasional seiche activity (Cerralbo et al., 2015a). At large temporal scales the

water response consists of a combined effect of a gravitational circulation due to freshwater inputs and the residual effect of winds. During seiche activity maximum velocities in the node location reach 0.5 m/s. Numerical modelling excercises presented by Cerralbo et al. (2014) identify the antinode location near Trabucador beach shore, so that the expected velocities due to seiche activity are negligible. No measurements of currents are available at the Trabucador inner beach where bars are located but the currents were estimated with passive tracers during the field campaign of September 1988 (Falqués, 1989). With North wind of 7.3 m/s a maximum current of 0.30–0.35 m/s to the SW was observed over the crest of a bar with water depth of 0.05–0.1 m. The current was clearly favored by the breaking of the small waves over the bar. At the same time, at the deeps between the bars with 0.3–0.5 m depth currents of 0.15–0.20 m/s were observed. The maximum current in the opposite direction was about 0.2 m/s with 6.1 m/s wind from the S-SE.

~~2.2.~~2.2 The alongshore rhythmic morphological system

This system was first described by Falqués (1989) on the basis of field observations and the analysis of aerial photos and maps. Periodic visual inspections suggest that the rhythmic system is very persistent, although its prominence varies from very obvious to nearly nonexistent. The characteristic morphological units are shown in Fig~~ure~~. 2: bars and associated megacusps in Fig~~ure~~. 2a and large scale shoreline undulations in Fig~~ure~~. 2b.

~~2.2.1.~~2.2.1 *Bars and megacusps*

The inner Trabucador beach usually features many long finger transverse bars (LFTB). They are elongated with different orientations but most of them trend nearly perpendicular to the coastline (see Fig~~ure~~. 3) and they are typically rotated to the left with respect to shore normal viewing from the beach (an angle $\phi \approx 10 - 40^{\circ}$), i.e., they trend approximately to the W. Many of them reach the coastline and a megacusp develops at the attachment point (see Fig~~ure~~. 3c). Similar megacusps have been described by Evans (1939, 1938).

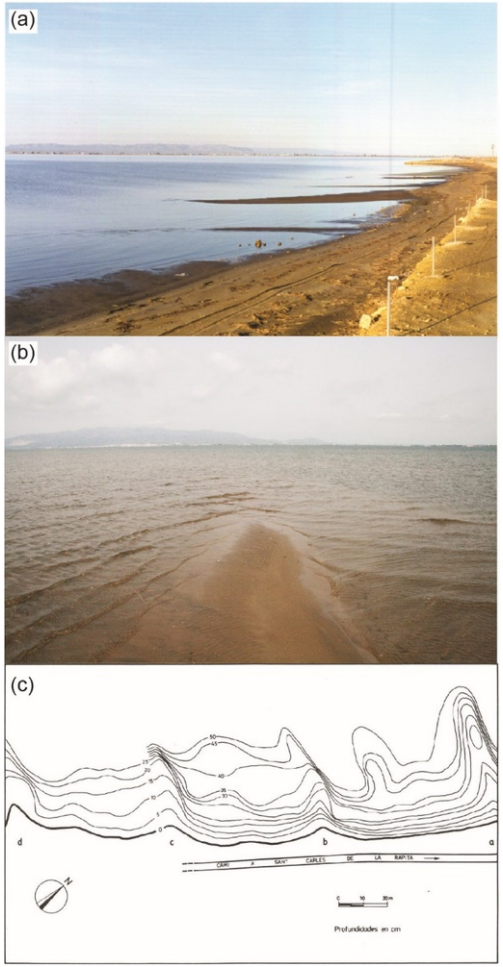

~~Figure 3~~Fig. 3 a) Transverse bars at low tide during the period 1986–1988. b) Transverse bar and the refractive wave focusing by it. c) Bathymetric map of a stretch of the Trabucador inner beach from August 1986 showing a series of 5 bars and 3 megacusps. The depths are in cm.

alt-text: Fig. 3

The length and alongshore spacing of the LFTB are of the same order of magnitude, the former tending to be larger than the latter. The spacing roughly ranges between 5 m and 100 m but is typically about 20 m. Their vertical relief can reach about 0.4 m. Typically, they are inter-tidal, becoming mostly emerged at low tide. As can be seen in the aerial photos, the whole bar system usually extends offshore into the Alfacs Bay across a significant portion of the shallow shelf. According to local fishermen, the bars have been there for, at least, the last 70 years. Indeed, they are already visible in an aerial photo of 1946.

Fig~~ure~~. 3c shows a bathymetric survey taken in August 1986 (Falqués, 1989) and displaying 4 main bars. The angle of the main bars with the shore normal is 14°, 24°, 19° to the left viewing from the beach. These bars have an asymmetric cross-bar profile steeper at the NE side and milder at the SW side. Their alongshore spacing is about 60–70 m. At the trough between two main bars there is a minor bar not connected to the shoreline and showing a weak opposite asymmetry. These smaller bars in between the larger ones (in length and in alongshore wavelength) are relatively common all along the beach. The bar system is dynamic and active. A clear indication was obtained in September 1988 when it was observed how the shape of a bar changed and how the crest migrated about 0.4 m within 20 ~~hours~~h during a daily fair weather conditions. The migration was consistent with the asymmetry in cross-bar shape, i.e., towards the steepest side. It was also observed how the ripples at the bar crest were formed, changed the shape and size and disappeared.

Although there are some differences (e.g., bar orientation or length vs spacing) we think these bars share important characteristics with those described by Evans (1938) as type 2. They were described as "large cusps which have their apexes

continuing out into the lake as a ridge of sand on the lake bottom. It was claimed they form on low energy beaches having a plentiful supply of sand and with a cross-shore bathymetric profile which is above the equilibrium profile, featuring a shallow terrace.

~~2.2.2.~~2.2.2 *Large scale shoreline undulations*

According to visual inspections of the aerial photos, in addition to the small amplitude shoreline undulations determined by the megacusps, there are larger shoreline undulations (see Fig~~ure~~. 2b). The apexes of these undulations sometimes coincide with the attachment of one of the largest bars. However, there is not a one-to-one relation between bars and large scale undulations since: i) there are also smaller bars with megacusps at the embayments and ii) sometimes the apexes of some undulations are apparently not associated to any bar. The wavelengths of these undulations are in the range 100~~-~~250 m, i.e., significantly larger than the typical alongshore spacing of the bars. Therefore, they can be identified as Km-scale shoreline sand waves although their wavelength is smaller than that of the similar features developing on open ocean beaches.

~~3.~~3 Methods

~~3.1.~~3.1 Image processing

This section describes the methodology we use to extract the information of the bar positions from the images along with the alongshore wavelengths using a Fourier analysis. Aerial orthophotos from the *Institut Cartogràfic i Geològic de Catalunya* (ICGC) during the period 1946~~-~~2014 are analyzed to assess the time evolution of the morphology and to obtain its alongshore wavelengths.

The available images are listed in Table 1. The shoreline is clearly visible in all of them but identifying the LFTB is not so straightforward. We have selected the central stretch of the Trabucador Beach (2 Km) where the bars are more visible. Usually, the bars can be detected from elongated patches with a colour that is in between the colour of the dry beach and the colour of the deeper water. In case of old black and white images, the dry beach appears in very light grey, the bars a bit darker and the troughs dark grey. In case of colour images, the dry beach appears in light yellow/brown, the bars in the same ~~colours~~colors but darker, and the deeper waters in blue. As can be seen in Table 1 the images have different resolution. Nevertheless, most of them are useful to locate both the bars and the shoreline undulations regardless of their resolution, as shown in Fig~~ure~~. 4a–b. However, the images from 1983 (Fig~~ure~~. 4c), 1996, 2000 (Fig~~ure~~. 4d) and 2004 are not good enough to capture the length of the bars due to the poor quality of the orthophoto, but can still be used to assess evaluate the shoreline undulations and the position of the bars.

Table 1 Orthophotos available in the ICGC with the corresponding resolution. The years that are not present in the table are years where the ICGC did not perform a flight in the Trabucador zone.

alt-text: Table 1

Year	Resolution (cm/px)	LFTB bars	Alongshore Und.
1946	100	YES	YES
1956	50	YES	YES
1983	50	YES	YES
1993	2500	NO	YES
1994	50	YES	YES
1996	2500	NO	YES
2000	50	NO	YES
2004	50	NO	YES
2007	50	YES	YES
2008	50	YES	YES
2009	25	YES	YES
2010	25	YES	YES
2011	25	YES	YES
2012	25	YES	YES

2013	25	YES	YES
2014	25	YES	YES

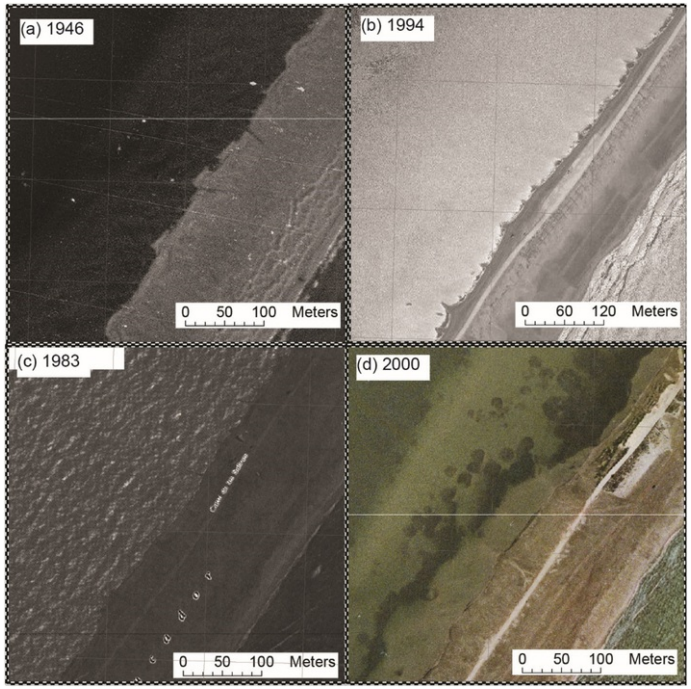

~~Figure 4~~**Fig. 4** Zoom in of four orthophotos during different years. a) b) high quality images; c) d) low quality images. Source: ICGC.

alt-text: Fig. 4

The method is based on tracking the sharp changes in colour associated to the bars and to the shoreline in between bars by a manual digitalization. In this way, an *Apparent Shoreline/Bar* signal (ASB) along the shore is obtained. This signal is, therefore, influenced mainly by the sea level and the light during the flight of the orthophoto. Thus, we do not attempt to extract the exact shoreline from the orthophotos, but a signal that is representative enough to capture the position of the main bars and the undulations present in the shoreline. In order to minimize the inherent errors of a manual digitalization, the same procedure was repeated several times, obtaining different signals from the same orthophoto. These sensitivity analysis on the manual profiling parameters showed no significant influences on the final results, since the differences between wavelengths were lower than 5 ~~meters~~m.

More specifically, the ASB signal is obtained from the images detailed in Table 1 as follows:

1. Manual profiling: images are loaded to a GIS specific software and a series of dots is manually assigned to the edges of the bar crests that are attached to the shoreline (identified as a sharp change in colour) and to the shoreline stretch in between bars (Fig~~ure~~. 5a). While there is typically a sharp change in colour across the bars that allows identifying relatively well both edges of a bar crest, the changes along the bar crests are quite gradual. Thus, the length of the bars is not well defined from the images and is not discussed here. According to the historical orthophotos, two concrete platforms were constructed along the inner beach and were present in the shoreline profile from 1994 to 2000. In order to minimize the noise of the final Fourier analysis, these platforms have been removed from the original signal.
2. Rotation: since the Trabucador barrier beach is North-East oriented (55°) and the Fourier transform needs a single-valued signal, the shoreline/bar line is rotated to approximate the mean shoreline along the x-axis, using a road that goes along the barrier beach (see Fig~~ure~~. 5b). However, the bars are still tilted towards the South-West and a single-valued signal is not obtained for all the bars. This creates some problems in the next step.
3. Interpolation: the Fourier analysis requires an equispaced digital signal. Thus, a new signal is obtained from the previous step by interpolating to an equispaced mesh. A linear interpolation with a spacing $\Delta x = 0.5$ m turned out to be satisfactory, although we should bear in mind that it introduces spurious peaks due to the slight inclination with respect to the normal direction of the Trabucador bar, see Fig~~ure~~. 5c–d. The sensitivity to different interpolation methods and grid spacing has also been examined in Fig~~ure~~. 5d and the best

results are provided by the linear interpolation.

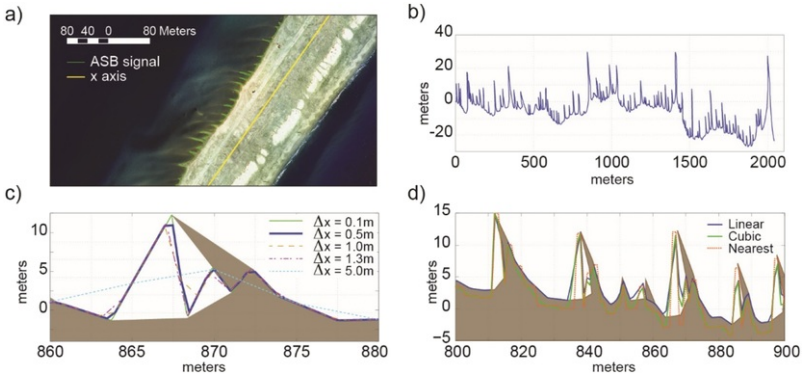

~~Figure 5~~**Fig. 5** Brown patch represents the beach contour given by the ASB signal. a) Raw ASB signal from the manual profiling. The yellow line indicates the direction of the x axis after rotation; b) Rotated ASB signal; c) Sensitivity analysis of the interpolated ASB signal as a function of the interpolation spacing, *Δx*. The different interpolated signals are shown in different colours.~~,~~; d) Sensitivity analysis of the ASB signal in function of the interpolation method. (For interpretation of the references to colour in this figure legend, the reader is referred to th web version of this article.)

alt-text: Fig. 5

It is important to point out that the present methodology incorporates significant noise below 10–15 m wavelength due to the spurious peaks of the ASB signal added during the interpolation step. Therefore, some existing peaks around 10 m will not be captured accurately using our methodology, as shown in Fig~~ure~~. 5d. The resulting ASB signals can be seen in Fig~~ure~~. 6.

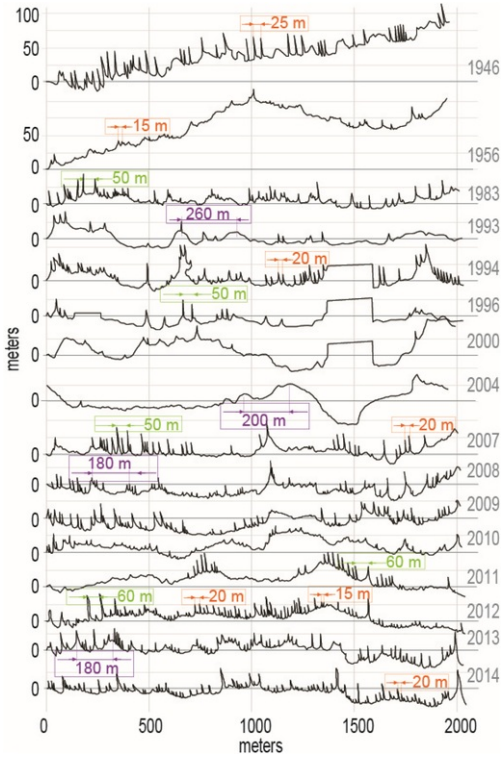

~~Figure 6~~**Fig. 6** Manual profiling results of the orthophoto images.

alt-text: Fig. 6

The Discrete Fourier transform of a continuous signal, $f(\xi)$, in the spatial domain is defined by:

$$f(\xi) = \frac{a_0}{2} + \sum_{n=1}^{\infty}\left[a_n \cos\left(\frac{2\pi}{\lambda_1} n\xi\right) + b_n \sin\left(\frac{2\pi}{\lambda_1} n\xi\right)\right] \quad \textbf{(1)}$$

where the coefficients are:

$$a_n = \frac{2}{\lambda_1}\int_0^{\lambda_1} f(\xi)\cos\left(\frac{2\pi}{\lambda_1} n\xi\right) d\xi$$
$$b_n = \frac{2}{\lambda_1}\int_0^{\lambda_1} f(\xi)\sin\left(\frac{2\pi}{\lambda_1} n\xi\right) d\xi \quad \textbf{(2)}$$

and the energy of each wavenumber is

$$|F_n| = \sqrt{{a_n}^2 + {b_n}^2} \quad \textbf{(3)}$$

where λ_1 is the fundamental wavelength and ξ is the spatial coordinate. The interpolation of the original ASB signal of the images provides a discrete signal and must be analyzed through a Discrete Fourier Transform (DFT) algorithm. Several algorithms can be found in the literature to compute the DFT and most of them are clearly affected by the sampling frequency and other inherent algorithm parameters. The present research uses the *Fast Fourier Transform* (FFT) assuming that valid wavenumbers will be below 1 m^{-1}. The results obtained after the FFT computation are very clear for high wavelengths (Figure 7a) but do not show robust peaks in the low wavelength range, see Figure 7b. Therefore, low wavelength scales are analyzed using Bartlett's Method. Bartlett (1948) estimates the power spectra by averaging the DFT results of N segments of the original signal. This is useful if the wavelength distribution is uniform along the signal but may smooth down some peaks that are present at a particular location of the signal. Therefore, Bartlett's results will enhance the existence of main wavelengths, present repetitively at the

different segments, compared to other secondary wavelengths.

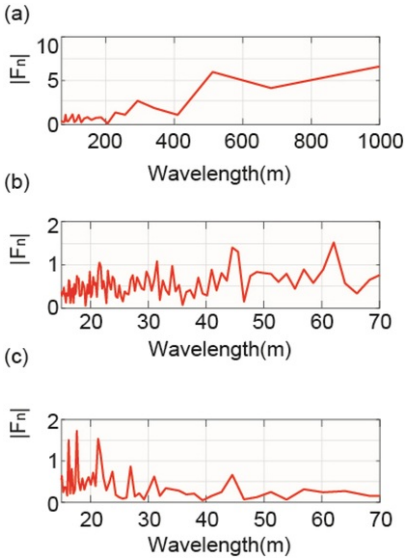

~~Figure 7~~Fig. 7 Methods used to compute the DFT using the signal from 2011. a) High wavelength results obtained after using the FFT method; b) Low wavelength results obtained after using the FFT method; c) Low wavelength results obtained after using the Bartlett's method.

alt-text: Fig. 7

Fig~~ure~~. 7c shows the results obtained using Bartlett's method by dividing the signal into five sections, which yields reliable peaks below 400 m wavelength. These results for low wavelengths can be compared to FFT results at the same scale by looking at Fig~~ure~~. 7b. It turns out that the original peak around 60 m with an FFT analysis, which is clearly visible in Fig~~ure~~. 7b is smoothed when the same signal is analyzed using Bartlett's method. However, the energy of the wavelengths around 20~~ meters~~m is reorganized in a single peak with the Bartlett's analysis. Sensitivity analysis performed to these two methods have shown that the most reliable results are obtained with the Bartlett's filter for low wavelengths and with the FFT algorithm for high wavelengths. Intermediate wavelengths behave as low wavelengths, bearing in mind that some important peaks may be smoothed down due to the assembling process associated to the Bartlett's filter.

~~3.2.~~3.2 Numerical modelling

This section presents the numerical modelling we have used to investigate the physical mechanisms that could have originated this system and/or could be driving its dynamics at present.

~~3.2.1.~~3.2.1 *Wave field*

Since wave measurements in front of this beach are not available, the SWAN model (Booij et al., 1999) is implemented for the Alfacs Bay and forced with representative winds to obtain wave height, direction and period. SWAN is a third generation spectral model, appropriate to estimate wave parameters in coastal areas and estuaries (see, for instance, Lin et al., 2002; Moeini and Etemad-Shahidi, 2007). This model is run in a stationary mode for two characteristic energetic wind conditions: 9 m/s from 220° (SW) and 15 m/s from 315° (NW). These conditions correspond to a representative wind of intense sea-breeze (typical during summer season) and measured peaks of offshore wind (typical during winter season), respectively (Cerralbo et al., 2015a; Grifoll et al., 2016).

~~3.2.2.~~3.2.2 *Morphodynamic instabilities~~.~~*

Coastal morphodynamic instabilities arise from feedbacks in the coupling between the hydrodynamics and the morphology through sediment transport in the coastal zone and can explain the genesis of alongshore rhythmic features in the morphology (see, e.g., Ribas et al., 2015). The Trabucador beach displays two different ranges of wavelengths: a) 5~~-~~100 m (typically about 20 m) corresponding to transverse bars/megacusps and b) 100~~-~~250 m corresponding to large scale shoreline undulations. Since both features coexist they should ideally come out of a single morphodynamic model that would also account for the possible interaction between them. However, such model is not yet available so that we will investigate each of them separately. This makes sense because transverse bars can exist in nature in absence of large scale shoreline undulations and vice versa. Therefore, their possible interaction is not essential for their formation.

According to the existing literature (e.g. van den Berg et al., 2012, Ribas et al., 2015, and references therein) the a) type could be driven by surf zone processes (alongshore gradients in wave breaking intensity, rip currents, meandering in the longshore current) while b) type could be driven by processes involving both the surf and shoaling zones (alongshore gradients in wave refraction and shoaling that cause gradients in alongshore sediment transport). As a result, a) and b) require different modelling approaches. The transverse bars/megacusps need a detailed description of the surf zone dynamics which can be done with the 2DH morfo55 model (Garnier et al., 2006). In contrast, the large scale shoreline undulations need a coupling between the surf and the shoaling zones whereas the details of the processes within the surf zone are not essential. Therefore, simplified models based on the one-line shoreline dynamics like the 1D-morfo model (Falqués and Calvete, 2005) are appropriate. We here down describe the basic concepts of these models. The details can be found in the provided references.

Morfo55 (Garnier et al., 2006) is based on the sediment conservation equation in two horizontal dimensions:

$$\frac{\partial z_b}{\partial t} + \frac{\partial q_x}{\partial x} + \frac{\partial q_y}{\partial y} = 0 \quad \textbf{(4)}$$

where t is time, x, y are Cartesian horizontal coordinates in the cross-shore and longshore directions, respectively, $z = z_b(x,y,t)$ is the bed level and (q_x,q_y) is the sediment flux integrated in the vertical (including a bed porosity factor). A number of different parameterizations of sediment transport can be used in the model but here we will use

$$\vec{q} = C\left(\vec{v} - \gamma \nabla h\right) \quad \textbf{(5)}$$

where $\vec{v}(x,y,t)$ is the vertically averaged mass transport current, $C(v,u_o)$ is a sediment stirring factor or total sediment load (Ribas et al., 2015), u_o is the wave orbital velocity at the bed, γ is the nondimensional downslope transport coefficient and h(x,y,t) is the bed level perturbation. The latter is the deviation with respect to the reference state (also called basic state), $z_b = z_{b0}(x)$, where all the variables are steady and alongshore uniform, i.e., the transverse bars are absent. In this formulation a total vertically integrated sediment concentration C is advected by the current (first term) and there is also a sediment flux that tends to smooth out the bathymetric perturbations (second term). The hydrodynamics includes the dynamics of the mean depth averaged currents and the mean sea level, described by momentum and mass conservation in 2 horizontal dimensions. Regarding the waves, their energy, wavenumber and direction over the evolving bathymetry are computed (from the dispersion relation, wave number irrotationality and wave energy conservation) but their phase is not resolved. A breaking criterion is included. From the currents and the waves the sediment flux is computed and its divergence provides the bed evolution through Equation (4). Thus, hydrodynamics and morphology are fully coupled. At $t = 0$ a small random bed level perturbation is added on top of the reference bathymetry and the model provides the time evolution of the morphology and the hydrodynamics for $t > 0$. An important limitation is that the swash zone is represented by a small vertical wall. Thus, the shoreline keeps on being rectilinear (y axis) during the simulation and megacusps cannot be explicitly represented. However, a shoal (deep) developing near the shoreline could be interpreted in reality as a megacusp horn (embayment between horns) formation. The lateral boundary conditions are of periodicity. At the offshore boundary, all deviations from the reference state tend to decay exponentially (radiation condition). At the shoreline, the cross-shore sediment flux and both components of the current are zero. The model has a number of inputs and parameters (see Garnier et al., 2006) and the most essential, are the size of the horizontal model domain, $0 \le x \le L_x$, $0 \le y \le L_y$ ($x = 0$ being the shoreline), the grid size, Δx, Δy (uniform over all the domain), the reference cross-shore beach profile, $z_b = z_{b0}(x)$, the initial perturbation and the parameters associated to wave breaking, sediment transport, bed friction and lateral momentum mixing. The wave parameters, significant wave height, H_s, peak period, T_p, and wave incidence angle with respect to the –x axis, θ, must be given at the offshore boundary ($x = L_x$). The main output is a number of files with the spatial distribution of all variables corresponding to selected times, $t = 0$, t_1, t_2,... t_n.

In the 1D-morfo model a small-amplitude sinusoidal undulation is imposed on a reference rectilinear shoreline ($x = 0$) being defined as:

$$x_s(y,t) = \frac{a}{2}\exp(\sigma t + iKy) + c.c \quad \textbf{(6)}$$

where a is the amplitude, K the alongshore wave number ($\lambda = 2\pi/K$), $\sigma = \sigma_r + i\,\sigma_i$ the complex growth rate and $c.c$ is the complex conjugate of the first term in the equation. Linked to the shoreline undulation, a perturbation in the bathymetry via a cross-shore shape function is considered. Regarding the unperturbed state, the main inputs of the model are the cross-shore reference beach profile $z_b = z_{b0}(x)$ and the given wave parameters, i.e., significant wave height, H_s, peak period, T_p, and wave incidence angle with respect to the –x axis, θ, at a certain depth. Regarding the perturbation, the main inputs are its alongshore wavelength, λ, the bathymetric shape function and the depth of its offshore reach, Dc. To compute σ, Eq. (6) is inserted into the one-line sediment conservation equation (Komar, 1998)

$$\frac{\partial x_s}{\partial t} = \frac{1}{\overline{D}}\frac{\partial Q}{\partial y} \quad \textbf{(7)}$$

where $\overline{D}$ is a mean depth of the morphodynamic active zone and $Q(H_b,\alpha_b)$ is the total alongshore sediment transport rate. It depends on the wave height H_b and the wave angle with respect to the local shore normal at breaking, α_b. Computing the left hand side of Eq. (7) is straightforward from Eq. (6) but estimating the right hand side requires calculating the perturbed H_b and α_b. This is done by linearizing (with respect to a) the equations describing refraction and shoaling over the perturbed bathymetry (linearizing the same equations of morfo55) and computing H_b and α_b numerically. The final goal of the model is computing the growth rate, σ, for each wavelength λ, to find the dominant wavelength, λ_M, i.e., that with larger $\sigma_r > 0$. This is the one that grows faster and that should therefore compare well with the observations.

4.4 Results

~~4.1.~~4.1 Image processing

The most apparent characteristics of the shoreline/bar lines from 1946 to 2014 (Fig~~ure~~. 6) is the large number of transverse bars, e.g., about 90 in 2 km stretch of coast in 2013, displaying a high complexity over this period. The bars are visible in most of the images and they are very striking in some of them, like those of 1946, 1983, 2009, 2012, 2013 and 2014. In some years the bars are ubiquitous over the whole beach stretch (e.g, 1946, 2012, 2013, and 2014). In these cases the spacing ranges from about 5 m to about 100 m, but the most frequent is around 20 m, clearly visible in 90% of the images with an average number of bars around 40. This is confirmed by the occasional inspections by the third author during the period 1986–2014. Their mean spacing is of the same order, for example, 22 m in 2013. But the bars can sometimes group in patches separated by gaps in between without the presence of bars (e.g., 2011). Then there is a relatively regular spacing in each patch that can differ slightly between patches. However, also in this case, the mean and the most frequent spacing are in the same range of about 20 m. Although the method of analysis (Section 3.1) does not allow determining the cross-shore length of the LFTB, their relative size can be estimated in some of the orthophotos so that the largest bars can be spotted. It is seen that smaller bars occur in between the largest ones and the spacing between the largest bars is larger than the spacing between the smaller ones, as it was already shown in the visual inspection in 1985–88 reported in the bathymetry shown in Fig~~ure~~. 3c. This is, bars separated about 50–60 ~~meters~~m are visible in 9 of the 16 years available with an average number of 15. Nevertheless, the bars are hardly visible in a few images, like those of 1993 or 2004. This could be due to either its absence in the field or to the bad quality of the images.

In addition to the LFTB and the associated megacusps, the shoreline itself is never straight and displays undulations that change in time and possess numerous length scales. A wavelength about 200 m is very clear in 2013 and is relatively common in other images too (70% of images with an average number of 10 bars following this characteristic wavelength). Larger scale undulations displaying alongshore wavelengths up to 500 m or more also show up, for example, in 1956, 2010 and 2011.

The results of the Fourier analysis of the ASB signal are shown in Fig~~ure~~. 8. Since this signal depends on the quality of the images plus the mean sea level at the moment of the orthophoto flight, the total energy of each peak depends also on these characteristics.

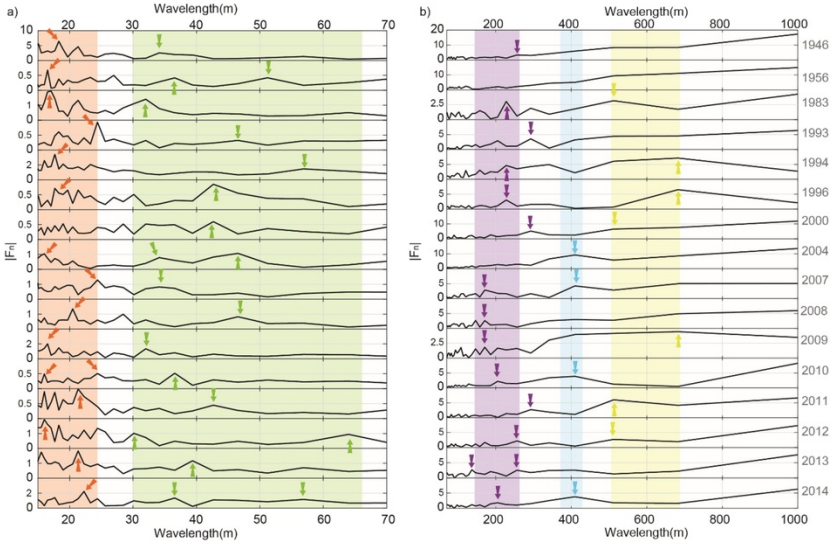

~~Figure 8~~**Fig. 8** a) Low wavelength results analyzed using Bartlett's method. b) High wavelength results analyzed using FFT. Notice that the vertical scale is not the same for the different images.

alt-text: Fig. 8

The low wavelength spectral analysis by using the Barlett's method, Fig~~ure~~. 8a, shows many energy peaks depending on the year. Sometimes there is a clear dominant one, e.g., L_b = 18 m in 1946, L_b = 24 m in 1993, L_b = 22 m in 2014. However, more frequently there are several peaks that are comparable in amplitude. What is quite clear is that the energy peaks can be mainly grouped in two bands:

- Short wavelength scale, in the range 15–25 m (red arrows in Fig~~ure~~. 8a). Peaks at this band appear in all the images except that of 2000, which is of bad quality. There is always a large concentration of spectral energy within this band regardless of the number of peaks. It is directly related to the most common spacing between transverse bars.

- Medium wavelength scale, in the range 30–65 m (green arrows in Figure 8a). It is related to the spacing between the largest LFTB. This is the spacing between LFTB in Figure 3c and was referred to in (Falqués, 1989).

The large wavelength spectral analysis by using FFT method is presented in Figure 8b. Consistently with the shoreline undulations which are visible in Figure 6, energy peaks from L = 150 to L = 700 m can be seen. We can group them in three bands:

- Wavelengths in the range 150–250 m (violet arrows in the plot). These are the most frequent peaks. They can be more clearly seen in 1983, 1996 and 2000, but are present in almost all the images.
- Wavelengths about 400 m (cyan arrows in the plot). They are less frequent but when they appear they are dominant, for example in 2014.
- Wavelengths in the range 500–700 m (yellow arrows in the plot). They are relatively common and sometimes they can be dominant, for example in 1996, but the peaks tend to be very smooth. They are linked to the overall morphology of the Trabucador barrier beach. Although the validity of the FFT for these length scales so close to the domain length is arguable, such wavelengths show up for the large scale undulations in Figure 6, for example in 1956 or in 2000.

We conclude that even though the morphology is highly dynamic and variable in time, it turns out that the rhythmic system itself is very persistent with wavelength bands that are quite robust. A sensitivity analysis on the interpolation and FFT methods concluded that wavelengths below 10 ~~meter~~m were clearly influenced by both.

~~4.2.~~4.2 Numerical modelling

~~4.2.1.~~*4.2.1 Wave field*

Figure 9 shows the wave field obtained by the SWAN numerical model in both scenarios, intense SW breeze (9 m/s from 220°) and strong NW wind event (15 m/s from 315°). Maximum wave heights of $H_s \approx 0.7$ m and $H_s \approx 0.4$ m are observed, respectively. However, to apply the morphodynamic models the wave parameters in shallow water close to the beach are necessary. At a water depth $D = 1.6$ m at the center of the study area, $H_s \approx 0.25$ m, incidence angle with respect to north ≈ 260°, peak wave period $T_p \approx 2.6$ s and average absolute period 1.8 s is obtained in case of the SW breeze. As the orientation of the Trabucador beach with respect to the north is 36°, the inner shore-normal trends to 306° and the wave incidence angle with respect to it is $\theta \approx 46°$. For the NW event $H_s \approx 0.65$ m, $T_p \approx 3$ s and the incidence angle with respect to north ≈305°, i.e., nearly shore-normal.

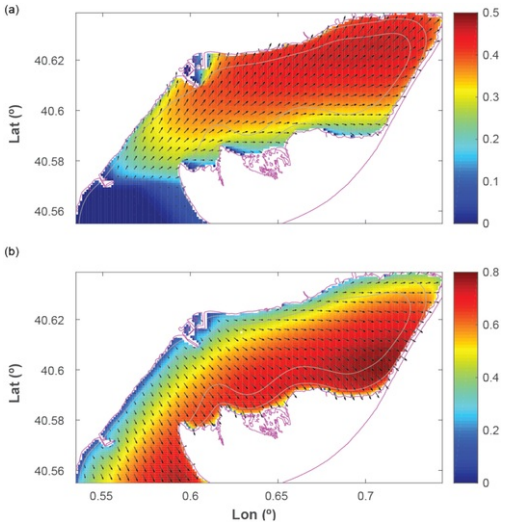

~~Figure 9~~**Fig. 9** Spatial distribution of the significant wave high and wave direction of propagation (black arrows). (a) case for 220° (clockwise positive) wind direction case for SW wind direction and 9 m/s wind intensity (b) case for NW wind direction and 15 m/s wind intensity. Notice that the ~~color~~colour bar limits is not the same for the different images.

alt-text: Fig. 9

~~4.2.2.~~*4.2.2 Transverse bars/megacusps*

The cross-section asymmetry of the bars suggests the presence of an alongshore current directed to the NE, i.e., generated from SW wind/waves. Existing literature on the genesis of transverse bars by morphodynamic instability (see, e.g., Ribas et al., 2015) shows that in this case up-current oriented bars can develop. Thus, the observed bar asymmetry and orientation suggest that SW wave events could force the driving mechanism for these bars and this is our working hypothesis. The cross-shore and longshore lengths of the model domain are $L_x = 150$ m and $L_y = 100$ m, respectively. Even though the morphodynamics takes place only close to the shoreline, let say, $0 \leq x \leq 50$ m, the correct resolution of the hydrodynamics requires a quite wider domain in the cross-shore direction. The grid size is $\Delta x = \Delta y = 0.5$ m. Random initial perturbations in bed level are considered with a total amplitude from top to valley of 0.01 m. The wave parameters at the offshore boundary ($x = L_x$, $D = 0.7$ m) are constant and set to $H_s = 0.28$ m, $T_p = 2.5$ s and $\theta = 30°$, which are in the range of those obtained from SWAN simulation in the case of SW breeze. The breaking parameter is $\gamma_{bs} = 0.5$ and standard values are used for the bed friction and lateral momentum mixing parameters (Garnier et al., 2006). Regarding sediment transport we here use a constant stirring factor $C = 0.001$ m^3/m^2 and the downslope transport factor is $\gamma = 0.3$. These are standard values that are suggested by previous studies (see, e.g., Garnier et al., 2006).

The time evolution of the bed level perturbation, h(x,y,t), from $t_o = 0$ to $t = 37$ h is shown in Figure 10a. After some 15 hours, the bed has self-organized into an alongshore rhythmic pattern encompassing subtle up-current oriented oblique bars with a wavelength $\lambda = 10$ m. The +0.01 m depth contour (bounding the yellow area in the plot) could very well represent the shore attachments of the observed bars at el Trabucador. Subsequently, a clearly nonlinear process with merging of some bars develops and a second wavelength of $\lambda \approx 33$ m shows up. For a while both wavelengths compete (e.g., $t \approx 28$ h) and the model morphology seems to reproduce the observed mix of larger bars with minor bars in between. This is a typical nonlinear phenomenon which is a result of various competing instability modes and in this case it shows a cascade towards larger wavelengths as time passes as it is observed by Ashton et al. (2001) for larger scale coastal features. For $t \approx 35$ h the larger wavelength is clearly dominant and in a relatively short time the amplitude of the bars has grown significantly, from $A \approx 0.01$ m to $A \approx 0.09$ m, where A = max(h) – min (h). For $t = 37$ h this pattern with clear up-current oriented bars persists and the amplitude growths to $A \approx 0.10$ m but the model run blows up because one of the bar crests gets out of the water next to the shoreline (pointing to a megacusp formation), a process which is not resolved by the model. The blow-up can be avoided by increasing γ, but we think that the similitude of the pattern we obtain with the observed bars and the simulation time of 37 hours are enough to show that the genesis of the observed bars can by caused by the feedback described by the model. By comparing $t = 34.5$ h with $t = 37$ h, it is seen that the bars move downcurrent at a rate of 2.8 m/h. However, the conditions of such observations were much less energetic than the SW breeze event we are assuming for morfo55. Figure 10b presents a zoom of the 'final' bar pattern for $t = 37$ h where the along-current asymmetry of the cross-bar bed profile is clearly visible, the lee of the bars being steeper than the stoss like it is seen in the bathymetric map of Figure 3c. However, the angle of the model bars with respect to the shore-normal is about 50° whereas in nature it is variable but tends to be less, e.g., about 36° for some of the bars in 2012 shown in Figure 1 or about 20° in the bathymetric map in Figure 3c (see also Figure 2a). Figure 10b also shows the final total bathymetry, i.e., $z_b = z_{b0}(x) + h(x,y,t)$. The alongshore asymmetry is quite striking and despite the simplicity of the model the depth contours bear some resemblance with the bathymetric lines in Figure 3c. Importantly, the two wavelengths that come out of the model run, $\lambda = 10$ m and $\lambda = 33$ m fit very well in the observed wavelength range.

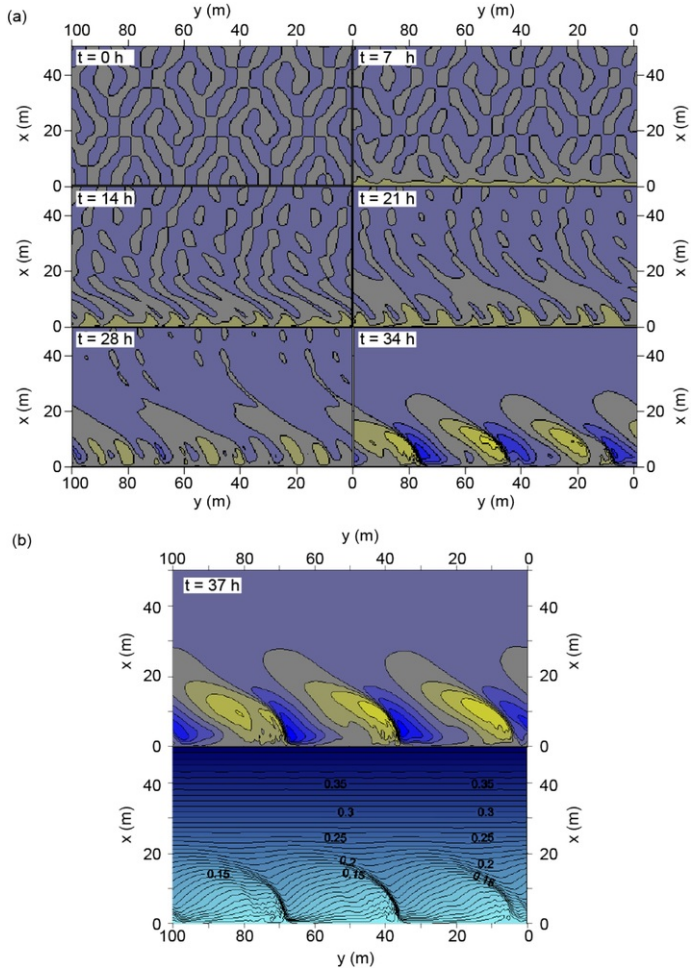

~~Figure 10~~Fig. 10 Modelling the formation of transverse bars out of initial random noise with morfo55 for strong breeze from the SW. Wave parameters are Hs = 0.28 m, Tp = 2.5 s, θ = 30°. Maximum bed level differences for the initial perturbation are 0.01 m. For each plot, the shoreline is at the bottom, NE is at the right and SW is at the left. (a) The bed level perturbation with respect to the reference alongshore uniform mean bathymetry is shown. Yellow ~~color~~colour corresponds to shoals, blue ~~color~~colour corresponds to deeps with maximum bed level difference of 0.1 m. (b) Upper panel: final (after 37 h) morphology of the bars for the morfo55 run (contours and colors as in a); Lower panel: total bed level contours (reference + perturbation). The depth increment between contours is 0.01 m, the labels are in m (notice that for computational reasons the shoreline is not at water depth D = 0 but at D = 0.03 m). (For interpretation of the references to colour in this figure legend, the reader is referred to the web version of this article.)

alt-text: Fig. 10

~~4.2.3.~~4.2.3 Large scale shoreline undulations

It is well known that Km-scale shoreline sand waves can form from a shoreline instability driven by high-angle waves (Ashton et al., 2001). The waves generated by the intense SW breeze events have very high incidence angles with respect to the inner Trabucador shoreline at the center of the Alfacs bay. This motivates applying the 1D-morfo model to investigate whether that instability could drive the large scale shoreline undulations for such wave conditions. NE winds could also generate high-angle waves thereby inducing this instability. We do not consider them because i) they are less frequent and ii) they would reinforce the effect of the SW waves just modifying the shape of the undulations and their alongshore translation (see, e.g., van den Berg et al., 2012). Regarding the reference cross-shore bathymetric profile, Fig~~ure~~. 11a shows bathymetric data provided by Dr. Guillén (personal communication) and its analytic approximation which is used for the model.

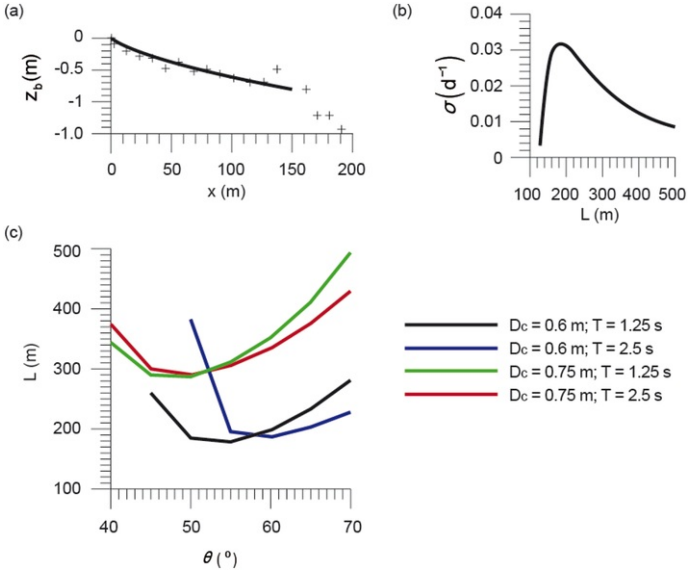

~~Figure 11~~Fig. 11 Modelling large scale shoreline undulations with 1D-morfo for strong breeze from the SW. (a) cross-shore mean bathymetric profile, observed (diamonds) and analytical approximation used by 1Dmorfo (thick line). (b) typical instability curve, growth rate as a functio of wavelength, showing a dominant wavelength about 180 m. The parameters are H_s = 0.25 m, T_p = 1.25 s, θ = 50° with D_c = 0.6 m. (c) dominant wavelength as a function of wave angle, θ, for various D_c and T_p and for H_s = 0.25 m. Below θ = 40° there is no undulation growth.

alt-text: Fig. 11

The depth of closure, D_c, is an important parameter for shoreline sand wave formation over which there is some uncertainty (Falqués et al., 2017). From the morphology of the inner Trabucador beach encompassing first a shallow terrace up to 0.7 m depth and then a steep break towards the Alfacs bay (Figure 1), a value $D_c \sim 0.7$ m seems reasonable. More importantly, the aerial photos reveal that the alongshore rhythmic bathymetry extends up to water depth of this order and then disappears (Figure 1). Thus, we here explore two values, $D_c = 0.6$ m and $D_c = 0.75$ m. Regarding the shape of the bathymetric perturbation a linear decay in bed level from 1 at the shoreline to 0 at D_c is considered. The effect of different shape functions on model shoreline sand wave formation is discussed in Idier et al. (2017). Regarding the wave conditions we use the SWAN outputs in case of SW breeze as a reference. The wave height is a robust output of the SWAN model so that we fix H_s = 0.25 m and we explore T_p from 2.5 s down to 1.25 s. Regarding the wave angle, it is advisable to explore a wide range including the output of SWAN (in order to obtain a threshold angle for the instability) so that we consider wave angles from θ = 20° up to θ = 70° (at D_c = 1.6 m). Finally, concerning the wavelength of the undulations we examine the range 100 m ≤ λ ≤ 500 m. For that range of wavelengths, the instability curves (growth rate σ_r as a function of λ) look like the one represented in Figure 11b for H_s = 0.25 m, T_p = 1.25 s, θ = 50° and D_c = 0.6 m. In this case, the maximum growth rate is σ_r = 0.032 d^{-1} which defines the dominant wavelength, λ_M = 180 m. This means that the characteristic time formation of those undulations is about $\sigma_r^{-1} \approx 31$ d assuming constant wave conditions. As shown in Figure 11c, the dominant wavelength has been explored as a function of θ for various D_c and T_p. First it is seen that the formation of shoreline undulations needs a minimum wave angle in accordance with high-angle wave instability theory (Ashton et al., 2001; Falqués and Calvete, 2005). For T_p = 1.25 s, this threshold angle is about 40° for D_c = 0.75 m and 45° for D_c = 0.6 m. For T_p = 2.5 s and D_c = 0.6 m it is 50°. It is found that the dominant wavelengths range between 180 and 500 m and they increase with D_c. For D_c = 0.6 m and excluding those corresponding to the angles near the threshold, they are in the range 180–280 m. For D_c = 0.75 m they are in the range 290–500 m. Therefore, the range of variability of these wavelengths as a function of the wave parameters matches quite well the range of large alongshore length scales revealed by the image processing presented in Section 4.1. In particular, the range 150–250 m seems quite well captured by the D_c = 0.6 m model results. The wavelengths about 400 m could be roughly associated to D_c = 0.75 m. Importantly, the existence of a threshold angle for shoreline instability rules out the possibility that NW wind events could generate such large scale undulations.

~~5.~~5 Discussion and possible driving mechanisms

~~5.1.~~5.1 Morphodynamic characteristics of the observations~~.~~

Previously, it is important to identify some of the characteristics of the morphological system that can provide clues into the driving processes:

- The system is nowadays active, it is not relict. This is very obvious from Figure 6. However, the field observations during the period 1986 to present are very scarce and the aerial orthophotos are available once a year at most. Also, it is sometimes difficult to ascertain whether the bars are not there or they are simply not visible. Thus, with the available information it is impossible to accurately assess the time variability of the system and try to link it to particular meteorological events.

- The range of wavelengths (Section 4.1). For the transverse bars/megacusps it is 15–65 m and the overall most common is about 20 m. For the large-scale undulations it is about 150–400 m but the most typical wavelengths are about 150–250 m.
- Refractive wave focusing by the bars. As shown in Figure 3b, the small waves approaching the bars strongly refract, the wave crests turn towards the bar crest and cross the wave crests coming from the other bar flank. This creates a zone with small breakers over the bar crest and a quite strong onshore current over the bar. Currents of about 0.35 m/s and sediment mobility (mainly bed-load) associated to it have been observed by Falqués (1989). This is a very striking and persistent process on this beach. This process was clearly described by Niederoda and Tanner (1970) and was suggested to be one of the driving mechanisms of some transverse bars.
- Obliquity and orientation. According to the aerial photos the bars are not shore normal but oblique, i.e., they are typically rotated to the left viewing from the shore an angle ranging from 10° to 40°.
- Alongshore asymmetry of the cross-bar bed profile. A bathymetric map taken in 1986 (Figure 3c) shows an asymmetric profile of all the bars, steeper at the NE flank of the bars and milder at the SW flank (except a minor one). Additional bathymetric observations are not available so that we do not know whether this is always the case or not. From the distribution of dark and light colors in the aerial photos some symmetry/asymmetry can be sometimes guessed and it seems that the asymmetry observed in Figure 3c does not always occur.

5.2.5.2 Transverse bars

In Section 4.2.2 we have seen how the morfo55 model describes the self-organized formation of transverse bars out of initial bathymetric noise during some 35 hourshours of strong SW breeze (9 m/s). Of course, 35 hourshours of such constant wind is unrealistic, but at least 6 hourshours a day is quite common during many summer days. This means that the bars could form during a few weeks of common summer breeze regime at El Trabucador. The observed range of wavelengths, the oblique orientation, the alongshore translation and even the presence of different bar sizes are captured by the model. A quantitative comparison on the alongshore celerity is impossible without knowing the wave conditions for the observed translation. According to the morfo55 equations, the physical processes that are essential for the formation of the bars would be as follows. The SW wind drives waves incoming obliquely to the Trabucador beach from the W. The breaking of these waves drives a longshore current to the NE. The incipient bars act on the current in two ways: a) they cause a meandering of the current, seaward at the crests and shoreward at the troughs (bedflow effect) and b) due to the refractive focusing, there is more wave energy hence more breaking over the crests and less wave energy hence less breaking at the troughs (bedsurf effect). This causes gradients in wave radiation stresses and in wave-setup that also alters the longshore current. Morfo55, then, computes the perturbed sediment flux and it turns out that the gradients in sediment flux create sediment deposition at the crests and sediment erosion at the troughs thereby a positive feedback occurs. The details of the physical mechanism that can drive up-current oriented transverse bars had been generically studied by Ribas et al. (2003), Garnier et al. (2006) and Ribas et al. (2015). Regarding its specific application to nature, Ribas et al. (2012) found that the medium energy transverse finger bars observed at Noordwijk beach, the Netherlands, could be explained by this mechanism. However, the present research is the first time this feedback mechanism is found to drive long finger transverse bars (LFTB). Although the physical mechanism is similar to Ribas et al. (2012) there are a number of differences with the present study (see Section 1). The most essential are i) the level of wave energy, ii) whether they are ephemeral or persistent and iii) whether there is a shore-parallel bar or not. Moreover, the present study uses nonlinear morphodynamic time evolution while Ribas et al. (2012) use linear stability analysis. LFTB bars have also been observed at El Puntal beach, Santander (Cantabria, Spain) by Pellón et al. (2014). However, there are two important differences with the Trabucador system: those bars are down-current oriented and the tidal range is significant, up to 5 m. Moreover, a morphodynamic modelling of their formation is not available so that their formation mechanism is still unknown.

The driving force for the current in the present setup for the morfo55 model is just wave breaking. Other processes could help in driving a current to the NE at El Trabucador beach. First of all, the SW wind itself could do this job. Pellón et al. (2014) compared the wind and the wave forces on the water for a transverse bar system in a tidal low-energy beach and concluded that they were of the same order of magnitude. Cerralbo et al. (2016) investigate the water circulation pattern in Alfacs Bay using a fully 3D ocean numerical model. Their numerical experiments showed a current jet in the inner shore of the Trabucador beach associated to NW wind. Also, less frequent NE winds may be the origin of a southwestward current as a local response to the wind. As far as we know, there is only one published study on morphodynamic instabilities induced by currents partially driven by wind in the surf zone (Ribas et al., 2012). Although the environment is quite different from El Trabucador (open ocean barred beach, medium wave energy conditions) that study suggests that wind effects could reinforce the self-organization process presented in Section 4.2.2. Certainly, more detailed observations are needed along with specific modelling studies on morphodynamic instabilities generated by partially wind-driven current.

The refractive wave focusing and breaking by the bars was pointed out as the main formation mechanism for LFTB bars by Niederoda and Tanner (1970). This effect is included in our morfo55 simulation (bedsurf effect) but in combination with the longshore current deflection (bedflow effect) which essentially occurs in case of oblique wave incidence. Since the Trabucador bars are oblique and frequently asymmetric they very likely have formed under the action of a current. In contrast and according to Niederoda and Tanner (1970), the bars which are primarily formed by the refractive wave focusing can emerge even in case of normal wave incidence being shore-normal and cross-bar symmetric. Thus, we conclude that the present bars are not formed only by the refractive wave focusing but by the combination of both this process and the longshore current interaction with the bars.

At this point, we wonder which could be the possible role of NW wind events on the bars. A model study similar to that carried out for SW wind is beyond the scope of the present work and is left for future research. In that case, the wave incidence is nearly shore-normal and the refractive wave focusing could play a role in initiating bar formation without cross-bar asymmetry and with a nearly shore-normal orientation, according to Niederoda and Tanner (1970). Also, the NW wind could contribute to reshape the bars once formed during SW wind events. Thus, we finally conclude that the SW breeze would be the primary cause of the transverse bars although there could be some

influence of NW wind events that still remains unknown.

We should finally mention an important occasional process that takes place at the Trabucador barrier beach. During severe storms from the E or NE the Trabucador barrier beach is sometimes flooded and breached (Gracia et al., 2013). Overwash fans can then appear and they perhaps might act as an initial perturbation that would initiate the feedback mechanisms between morphology and hydrodynamics. The self-organized processes would later on create the long finger transverse bars and induce the alongshore periodicity. Since the bars are much thinner than the overwash fans it is unlikely that these fans were the seed for the bars.

~~5.3.~~5.3 Large-scale shoreline undulations

In Section 4.2.3 we have seen that if we ignore the transverse bars and the details of the surf zone morphology a positive feedback between hydrodynamics and the smoothed morphology can still occur at wavelengths one order of magnitude larger than transverse bars if the SW wave incidence angle is large enough. This feedback is based on the alongshore gradients in the cross-shore averaged bed elevation when the alongshore gradients of total longshore transport cause deposition at the shoals of the averaged bathymetry and erosion at the depressions. These gradients occur because of the alongshore variations in wave refraction and shoaling in the shoaling zone, which must be coupled to the surf zone. Depending on some parameters, the 1D-morfo computations give a range of wavelengths $\lambda \sim 180$–500 m which matches quite well the range of the observed large scale shoreline undulations. We thus conclude that high-angle wave instability for SW breezes could provide a plausible explanation for the large scale shoreline undulations.

~~6.~~6 Concluding remarks

The analysis of the aerial orthophotos and direct observations of the Trabucador beach have shown that the inner side commonly features an intricate and complex morphology that is alongshore rhythmic at a number of different lengthscales. The most apparent morphological unit is the long finger transverse bars (LFTB). These bars typically attach to the shoreline by a megacusp and both the mean and the most frequent alongshore spacings are about $L = 20$ m. The spectral analysis of the digitalized signals shows many peaks with inter-annual variability. However, there is always a significant concentration of peaks at the 15–25 m band. This preferent lenghscale is also confirmed by the in situ observations. Therefore, we conclude that the dominant alongshore spacing of the LFTB is typically about 20 m. The spectral analysis also shows (less frequent) peaks in the band $L = 30 - 65$ m. Both the orthophotos and the direct observations show that they correspond to the spacing between the largest bars having minor bars in between.

Another morphological unit is the large scale shoreline undulations. Their systematic or rhythmic behavior is revealed by the spectral analysis of the ASB signals and becomes very clear in some of the orthophotos. These undulations seem to be a different element not directly related to the LFTB. The corresponding alongshore wavelengths of those undulations range between about 150 m up to 700 m but the highest concentration of spectral peaks associated to them is around 200 m.

Although the morphology is highly dynamic, its main characteristics are persistent in time at least for the last 70 years. It is important to bear in mind that the lack of systematic experimental information has not yet allowed a detailed quantitative modelling of the development of the morphology during the pertinent observed meteorological and hydrodynamic conditions. Despite of it, we have used the 2DH morfo55 and the one-line linear stability 1D-morfo models to show that both the transverse bars/megacusps and the large scale shoreline undulations could be originated by the wave-driven alongshore current during the strong SW breezes. Thus, our model results suggest that the primary cause of the observed morphological system is the feedbacks between i) waves and currents and ii) morphology, through sediment transport during SW wind events. Although the influence of other weather conditions, in particular NW or NE wind, could be important we think it is not essential for the genesis of the morphology and is left for future research. Notwithstanding that our hypothesis that the main driver is SW wind events seems highly plausible, many aspects deserve further attention. From the modelling side, the role of NW wind events and the wind forcing on the current should be investigated. From the observational side, the state of the bar system should be monitored at least during one year to see whether bars are more prominent in summer or in winter, and to seek for possible correlation with meteorological events, in particular with prevailing SW winds. Also, direct measurement of waves and currents at the site would be highly desirable as a previous step of a more specific morphodynamic modelling. Other future works will be addressed to evaluate the significance of the results at methodological steps such as the coastline profiling or the Fourier analysis.

Uncited references

Calvete et al., 2001

Hallermeier, 1978

Acknowledgements

This research is part of the Spanish Government project CTM2015-631 66225-C2-1-P (MINECO/FEDER). The authors want to gratefully acknowledge Dr. J. Guillén for providing bathymetric data on the cross-shore beach profile at El Trabucador, Dr. R. Garnier for his support for the morfo55 runs and Dr. Cerralbo for providing numerical mesh information. The first author's funding comes from the research group

LIM/UPC.

References

Ashton A., Murray A.B. and Arnault O., Formation of coastline features by large-scale instabilities induced by high-angle waves, *Nature* **414**, 2001, 296–300.

Bartlett M.S., Smoothing periodograms from time series with continuous spectra, *Nature* **161**, 1948, 686–687.

Booij N., Ris R.C. and Holthuijsen L.H., A third-generation wave model for coastal regions: 1. Model description and validation, *J. Geophys. Res. Oceans* **104**, 1999, 7649–7666, https://doi.org/10.1029/98JC02622.

Bruner K.R. and Smosna R.A., The movement and stabilization of beach sand on transverse bars, Assateague Island, *Virginia. J. Coast. Res.* **5**, 1989, 593–601.

Calvete D., Falqués A., de Swart H.E. and Walgreen M., Modelling the formation of shoreface-connected sand ridges on storm-dominated inner shelves, *J. Fluid Mech.* **441**, 2001, 169–193, https://doi.org/10.1017/S0022112001004815.

Calvete D., Dodd N., Falqués A. and van Leeuwen S.M., Morphological Development of Rip Channel Systems: Normal and ~~N~~near Normal Wave Incidence, *J. Geophys. Res.* **110**, 2005.

Cerralbo P., Grifoll M., Valle-Levinson A. and Espino M., Tidal transformation and resonance in a short, microtidal Mediterranean estuary (Alfacs Bay in Ebre delta), *Estuar. Coast. Shelf Sci.* **145**, 2014, 57–68.

Cerralbo P., Grifoll M. and Espino M., Hydrodynamic response in a microtidal and shallow bay under energetic wind and seiche episodes, *J. Mar. Syst.* **149**, 2015a, 1–13, https://doi.org/10.1016/J.JMARSYS.2015.04.003.

Cerralbo P., Grifoll M., Moré J., Bravo M., Afif A.S. and Espino M., Wind variability in a coastal area (Alfacs Bay, Ebro River delta), *Adv. Sci. Res.* **12**, 2015b, 11–21.

Cerralbo P., Espino M. and Grifoll M., Modeling circulation patterns induced by spatial cross-shore wind variability in a small-size coastal embayment, ~~*Ocean Model.*~~*Ocean Model* **104**, 2016, 84–98, https://doi.org/10.1016/J.OCEMOD.2016.05.011.

Coco G. and Murray A.B., Patterns in the sand: ~~F~~from forcing templates to self-organization, *Geomorphology* **91**, 2007.

Coco G., Huntley D.A. and O~~'~~Hare T.J., Investigation of a self-organization model for beach cusp formation and development, *J. Geophys. Res.* **105**, 2000, 21991–22002.

Deigaard R., Drønen N., Fredsoe J., Jensen J.H. and Jørgensen M.P., A morphological stability analysis for a long straight barred coast, *Coast. Eng.* **36**, 1999, 171–195.

Dodd N., Stoker A., Calvete D. and Sriariyawat A., On Beach Cusp Formation, *J. Fluid Mech.* **597**, 2008, 145–169.

Evans O.F., The classification and origin of beach cusps, *J. Geol.* **46**, 1938, 615–627.

Evans O.F., Mass transportation of sediments on subaqueous terraces, *J. Geol.* **47**, 1939, 325–334.

Falqués A., Formación de Topografía a rítmica en el Delta del Ebro, *Rev. Geofísica* **45**, 1989, 143–156.

Falqués A. and Calvete D., Large scale dynamics of sandy coastlines. Diffusivity and instability, *J. Geophys. Res.* **110**, 2005.

Falqués A., Coco G. and Huntley D.A., A mechanism for the generation of wave-driven rhythmic patterns in the surf zone, *J. Geophys. Res.* **105**, 2000, 24071–24088.

Falqués A., Ribas F., Idier D. and Arriaga J., Formation mechanisms for self-organized km-scale shoreline sand waves, *J. Geophys. Res. Earth Surf.* 2017, 122.

Garnier R., Calvete D., Falqués A. and Caballeria M., Generation and nonlinear evolution of shore-oblique/transverse sand bars, *J. Fluid Mech.* **567**, 2006, 327–360.

Garnier R., Calvete D., Falqués A. and Dodd N., Modelling the formation and the long-term behavior of rip channel systems from the deformation of a longshore bar, *J. Geophys. Res.* **113**, 2008.

Gelfenbaum G. and Brooks G.R., The morphology and migration of transverse bars off the west-central Florida coast, *Mar. Geol.* **200**, 2003, 273–289.

Gracia V., Garcia M., Grifoll M. and Sánchez-Arcilla A., Breaching of a barrier under extreme events. The role of morphodynamic simulations, *J. Coast. Res.* **65**, 2013, 951–956.

Grifoll M., Aretxabaleta A.L. and Espino M., Shelf response to intense offshore wind, *J. Geophys. Res. Oceans* **120**, 2015.

Grifoll M., Navarro J., Pallares E., Ràfols L., Espino M. and Palomares A., Ocean-atmosphere-wave characterisation of a wind jet (Ebro shelf, NW Mediterranean Sea), *Nonlinear Process. Geophys.* **23**, 2016, 143–158.

Guillén, J., Acosta, J., Chiocci, F.L., Palanques, A., 2017. Atlas of Bedforms in the Western Mediterranean. Springer International Publishing, Cham. doi:https://doi.org/10.1007/978-3-319-33940-5.

Hallermeier, R.J., 1978. Uses for a calculated limit depth to beach erosion, in: Coastal Eng. 1978. Am. Soc. of Civ. Eng., pp. 1493–1512.

Holman R.A. and Bowen A.J., Bars, bumps, and holes: models for the generation of complex beach topography, *J. Geophys. Res.* **87**, 1982, 457–468.

Idier D. and Falqués A., How kilometric sandy shoreline undulations correlate with wave and morphology characteristics: preliminary analysis on the {A}tlantic coast of {A}frica, *Adv. Geosci.* **39**, 2014, 55–60.

Idier D., Falqués A., Rohmer J. and Arriaga J., Self-organized kilometre-scale shoreline sandwave generation: sensitivity to model and physical parameters, *J. Geophys. Res.* **122**, 2017.

Jiménez J., Sánchez-Arcilla A., Valdemoro H.I., Gracia V. and Nieto F., Processes reshaping the Ebro delta, *Mar. Geol.* **144**, 1997, 59–79, https://doi.org/10.1016/S0025-3227(97)00076-5.

Kaergaard K. and Fredsoe J., Numerical modeling of shoreline undulations part 1: ~~C~~constant wave climate, *Coast. Eng.* **75**, 2013, 64–76.

Khabidov, A., 2001. Transverse bars formation on a tideless beach, in: of Civil Engineers. Lund, S. (Ed.), Proceedings Coastal Dynamics 2001. ~~p~~Pp. 666–672.

Komar P.D., Beach {P}rocesses and {S}edimentation, Second. ed., 1998, Prentice Hall; Englewood Cliffs, N.J.

Konicki K.M. and Holman R.A., The statistics and kinematics of transverse bars on an open coast, *Mar. Geol.* **169**, 2000, 69–101.

Levoy F., Anthony E.J., Monfort O., Robin N. and Bretel P., Formation and migration of transverse bars along a tidal sandy coast deduced from multi-temporal Lidar datasets, *Mar. Geol.* **342**, 2013, 39–52.

Lin W., Sanford L.P. and Suttles S.E., Wave measurement and modeling in Chesapeake Bay, *Cont. Shelf Res.* **18**, 2002, 2673–2686.

Llebot C., Rueda F.J., Solé J., Artigas M.L. and Estrada M., Hydrodynamic states in a wind-driven microtidal estuary (Alfacs Bay), *J. Sea Res.* **85**, 2014, 263–276, https://doi.org/10.1016/J.SEARES.2013.05.010.

Moeini M.H. and Etemad-Shahidi A., Application of two numerical models for wave hindcasting in Lake Erie, *Appl. Ocean Res.* **29**, 2007, 137–145.

Niederoda A.W. and Tanner W.F., Preliminary study on transverse bars, *Mar. Geol.* **9**, 1970, 41–62.

Nienhuis ~~J. H.~~J.H., Ashton ~~A. D.~~A.D., Kettner ~~A. J~~A.J. and Giosan L., Large-scale coastal and fluvial models constrain the late Holocene evolution of the Ebro Delta, *Earth Surf. Dyn.* **5**, 2017, 585–603.

Palacin C., Martin D. and Gili J.M., Features of spatial distribution of benthic in fauna in a Mediterranean shallow-water bay, *Mar. Biol.* **110**, 1991, 315–321.

Pellón E., Garnier R. and Medina R., Intertidal finger bars at El Puntal spit, Bay of Santander, Spain: observation and forcing analysis, *Earth Surf. Dyn.* **2**, 2014, 349–361.

Pritchard, A., 1952. Estuarine Hydrography. Advances in Geophysics, vol. 1. Academic Press, Inc., New York, USA.

Ribas F. and Kroon A., Characteristics and dynamics of surfzone transverse finger bars, *J. Geophys. Res.* **112**, 2007.

Ribas F., Falqués A. and Montoto A., Nearshore oblique sand bars, *J. Geophys. Res.* **108**, 2003.

Ribas F., de Swart H.E., Calvete D. and Falqués A., Modeling and analyzing observed transverse sand bars in the surf zone, *J. Geophys. Res.* **117**, 2012.

Ribas F., Falqués A., de Swart H.E., Dodd N., Garnier R. and Calvete D., Understanding coastal morphodynamic patterns from depth-averaged sediment concentration, *Rev. Geophys.* **53**, 2015.

Shepard F.P., Revised nomenclature for depositional coastal features, *Bull. Am. Assoc. Pet. Geol.* **36**, 1952, 1902–1912.

Short A.D., Handbook of ~~b~~Beach and ~~s~~Shoreface ~~m~~Morphodynamics, 1999, John Wiley.

van den Berg N., Falqués A. and Ribas F., Modelling large scale shoreline sand waves under oblique wave incidence, *J. Geophys. Res.* **117**, 2012.